Extended Intranuclear Cascade model for pickup reactions induced by 50-MeV-range protons

Yusuke Uozumi[1a], Taiki Mori[1], Akifumi Sonoda[1] and Masahiro Nakano[2]

[1]*Kyushu University, Faculty of Engineering, 819-0395 Fukuoka, Japan*
[2]*Junshin Gakuen Univeersity, Faculty of Health Sciences, 815-8150 Fukuoka, Japan*

Abstract. The intranuclear cascade model was investigated to explain (p, dx) and (p, αx) reactions at incident energies of around 50 MeV. Since these reactions are governed mainly by the direct pickup process, the model was expanded to include exclusive pickup processes leading to hole-state-excitations. The energy of the outgoing clusters is determined with single-particle energies of transferred nucleons, the reaction Q-value, and the recoil of the residual nucleus. The rescattering of the produced cluster inside the nucleus is treated within the intranuclear cascade model. The emission angle is given by the sum of momentum vectors of transferred nucleons in addition to the deflection at the nuclear surface, which was introduced to explain angular distributions of elastic scattering. Double differential cross sections of reactions were calculated and compared with experimental data. The proposed model showed a high predictive power over the wide range of emission energies and angles. The treatment of the cluster transport inside the nucleus was also verified.

1 Introduction

The intranuclear cascade (INC) model is a powerful tool for predicting the double-differential cross sections (DDXs) of nuclear reactions. Many studies have been devoted to improving the accuracy of the INC model. As a consequence, the INC model has high predictive power at energies above a few hundreds of MeV, and plays an essential role in transport code systems for a variety of applications of engineering, medicine and fundamental sciences. In our previous works, the INC model has been successfully extended toward proton productions [1], and cluster productions [2,3] induced by protons of energies above 200 MeV or higher. More recently, we have successfully made extension of the INC model to the lower beam energies, around 50 MeV [4,5] by including collective excitations, trajectory deflections and barrier transmission coefficients. However, this improvement was carried out for only (p, $p'x$) reactions. For broadening the applicability of transport codes, further extension toward cluster production reactions below 100 MeV is crucial.

The INC model assumes that nuclear reactions can be described by sequential nucleon-nucleon collisions inside the nucleus, and that all nucleons other than the colliding pair behave as spectators. To describe the cluster production reactions, we have developed [2,3] the INC model to describe the knockout and the indirect pickup process by including nucleon correlations. These processes are responsible for reaction of incident energies above 100 MeV, and are suppressed strongly at the lower

[a] Corresponding author: uozumi@nucl.kyushu-u.ac.jp

energies. INC models developed elsewhere [6,7] incorporate the coalescence model, in which emitting particles within a certain phase space can be combined to form a cluster. The coalescence model is similar to the indirect pickup model, and cannot explain the high energy part of spectra where clusters have energies close to the incident beam energy. None of these models can be relied on to show a high predictive power at low beam energies. Since experimental observations of (*p*, *d*) reactions reveal discrete levels, which are attributed to the direct pickup process, up to at least 10 MeV of excitation energies, the inclusion of the direct pickup should therefore be a key to extending the INC model. It bears emphasis that all existing INC models lack explicit treatment of the direct pickup process. In the present work, we extend the INC model to (*p*, *dx*) and (*p*, *αx*) reactions of around 50 MeV.

The exclusive (*p*, *d*) reaction is explained as the direct single-neutron pickup process. The angular distribution of each *lj* transfer is calculated reasonably by the Distorted Wave Born Approximation (DWBA). Such discrete levels are observed up to about 10 MeV of excitations of residual nucleus. The continua at the higher excitations are not understood well. We assume that the higher excitation corresponds to the pickup from the deeply-lying shell orbit and the continua are the overlap of levels populated by intrinsic *lj* transfer.

The mechanism of the (*p*, *α*) reaction is unclear. The transitions to the ground state regions have been explained as the triton-pickup process in terms of DWBA analysis [8]. Although the mechanism of transitions to the excitation region higher than 5 MeV was concluded as the knockout process [8], the incident energies of 22 and 72 MeV are supposed to be too low to allow kinematically. Due to our INC prediction, *α* knockout is not observed at 70 MeV, and deuteron knockout appears barely. In the present study, we assume that these reactions are governed by the direct pickup process.

The rescattering of the cluster inside nucleus is treated within the INC framework. In order to check the particle transport inside the nucleus, DDXs for (*d*, *d'x*) and (*α*, *α'x*) reactions are also investigated. To describe the process, major modification of the INC model is necessary in order to include physical aspects neglected in previous studies. The evaporation stage is beyond the scope of this work.

2 Model

We assumed a two-stage model for nuclear reactions: the cascade and the evaporation processes. The cascade process is the first stage and described by the INC model, which assumes sequential *NN* collisions take place inside the target nucleus. The second stage is the evaporation process, which is the slow and statistical process. In the present work, we used the code GEM [9] for this stage. After the cascade process finishes, information of the residue nucleus is forwarded from INC to GEM.

2.1 Intranuclear cascade model

The prescription of the present INC model calculation is detailed in [1,3,4]; here we describe sole the essential points. The present model describes the time-development of the many-particle system. The target nucleus is considered to be a sphere with the nuclear radius R_0 and diffuseness *a.* They were given by $R_0 = \left(0.978 + 0.0206A^{1/3}\right)A^{1/3}$, and $a = 0.54$, respectively. Each nucleon is treated as spinless particles, and is given position and momentum randomly. However, target nucleons stay at the initial location before being struck out over the Fermi sea by the *NN* collision. The nucleon above the Fermi sea is assumed to travel inside the nucleus freely.

When two nucleons *i* and *j* approach to each other within a distance equivalent to the nucleon–nucleon cross section σ_{NN} [10]:

$$r_{ij} < \sqrt{\frac{\sigma_{NN}}{\pi}}, \tag{1}$$

they have a chance to undergo a collision. Pauli blocking is introduced to judge the collision phenomenologically using an operator $\hat{Q}$:

$$\hat{Q}|ij\rangle = [1-\Theta(E_i - E_F)][1-\Theta(E_j - E_F)]|ij\rangle, \quad (2)$$

where E_i and E_F are the energy of the nucleon after the collision and the Fermi energy, respectively. Θ denotes the unit step function. The scattering angle is determined stochastically to follow angular distributions of *NN* collisions in a way that energy and momentum are conserved.

In the INC model, DDX is assumed [4,5] to be

$$\frac{d^2\sigma}{dEd\Omega}(\theta,\varepsilon) = \sigma_{total}\frac{1}{2\pi\Delta E\Delta\cos\theta}P(\theta,\varepsilon), \quad (3)$$

where ΔE, $\Delta\cos\theta$, and σ_{total} are the bin width of the outgoing energy ε, the angle θ and proton-nucleus total reaction cross section, respectively. The form of proton emission probability P for (p, $p'x$) reactions, for instance, is given by

$$P(\theta,\varepsilon) = P_{def}^{in}(1+P_{CE})(G + GP_{NN}G + GP_{NN}GP_{NN}G + \cdots)P_{tr}P_{def}^{out}\big|_{\theta,\varepsilon}, \quad (4)$$

where G is the space development operator for energetic particles inside the target nucleus. The deflection function P_{def} has been determined to reproduce the angular distribution of elastic scattering, and gives deflection angle at the nuclear surface for both the entrance and the exit channels. P_{CE} is probability of the energy loss due to collective excitations of which cross sections are given in [5] as function of target mass number and incident proton energy. P_{NN} is *NN* collision probability and provides the energy and direction of scattered nucleon after the in-medium collision. P_{tr} gives barrier transmission probability [5] for the escaping proton.

2.2 Neutron pickup model for (p, d) reaction

To describe the direct (p, d) reaction process, the single-neutron pickup probability P_{np} was introduced. Since the knockout and the indirect pickup processes are suppressed strongly at incident energies around 50 MeV, the deuteron production is attributed to the direct pickup process. We assumed the pickup takes place when the incident proton enters the nucleus, and the deuteron emission probability is written by:

$$P^{pd}(\theta,\varepsilon) = P_{def}^{in}P_{np}(G + GP_{dN}G + GP_{dN}GP_{dN}G + \cdots)P_{tr}^{d}P_{def}^{out}\big|_{\theta,\varepsilon}, \quad (5)$$

where P_{tr}^{d} is the deuteron transmission probability, which is given by the unit step function at the Coulomb potential at a distance of $R_0 + 1.5$ fm from the center of the target nucleus. P_{dN} is a probability of the in-medium deuteron-nucleon collision. To transport the deuteron inside the nucleus, the deuteron is assumed to be a single elementary particle. The *d-N* cross section and the deuteron potential depth are assumed to be double for that of protons.

The deuteron energy E_d of the exclusive (p, d) reaction is given by

$$E_d = E_p - Ex + Q, \quad (6)$$

where E_p is the incident proton energy, Ex is the excitation energy of residual nucleus, and Q is the Q-value of the reaction, respectively. The kinematical correction is applied according to the emission angle and the excitation energy of residue. To introduce this relation into the INC model, we rewrite as

$$E_d = E_p - (E_F - E_n) + Q, \tag{7}$$

where E_F and E_n are the Fermi energy and the single-particle energy of the transferred neutron, respectively.

When the incident proton energy is 30 MeV or lower, the deuteron spectra are dominated by transitions to the ground state region. This means that the neutron in the outer shell orbit is picked up predominantly. With increasing the incident energy, pickup from inner shells occurs more frequently. It is supposed whether the transferred neutron is picked up from the surface orbit or not is the essential point to reproduce observed spectra over a wide incident energy range. Therefore, we introduce a weighting factor to emphasis the surface pickup contribution. The weighting factor was determined depending on the beam energy and the mass of target nucleus to fit the experimental energy spectra. The illustrations are shown in Figs. 1 (A) and (B) to explain the weighting factor for the choice of picked-up neutron from the two classes.

Angular distributions of (p, d) reactions depend on the transferred angular momenta. In the present model, we assume that the momentum direction of the produced deuteron is given by the added vector of the incident proton and the transferred neutron. When the deuteron leaves the nucleus, it undergoes deflection.

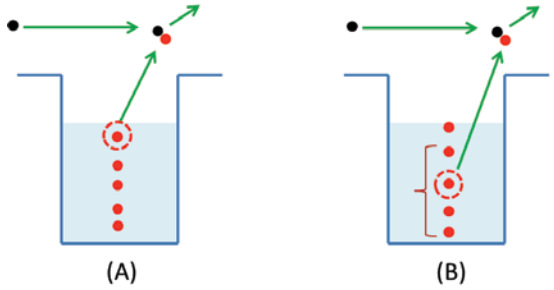

Figure 1. The two classes of the picked-up neutron in direct (p, d) reactions; (A) the surface one, and (B) one from the inner orbit.

2.3 Triton pickup model for (p, α) reaction

The pickup process for the exclusive (p, α) reaction is treated in a similar way to that for the (p, d) reaction. The α particle emission probability is given in the same way as eq.(5), but is displaced by triton pickup probability, α-N collision, and the α transmission efficiency. We assume that the residual nucleus is in a (ν^{-2}, π^{-1}) state and the α energy is given by

$$E_\alpha = E_p - (E_F - E_{n,1} - E_{n,2} - E_p) + Q, \tag{8}$$

where E_n and E_p is the single-particle energy of transferred neutron and proton, respectively. These energies of transferred nucleons, two neutrons and one proton, are chosen with a weighting factor, which was determined to fit the energy spectra depending on incident energy and mass of target nucleus. The class of the weighting factor is four as being illustrated in Fig. 2; (A) is the case to choose the most-surface-particles. (B) and (C) are the cases that include one or two particles lying in the deeper shell orbits, respectively. The case (D) includes no surface particles.

It is assumed that the momentum direction of the produced α particle is given by the added vector of the incident proton and the transferred nucleons. When the α particle leaves the nucleus, it undergoes deflection.

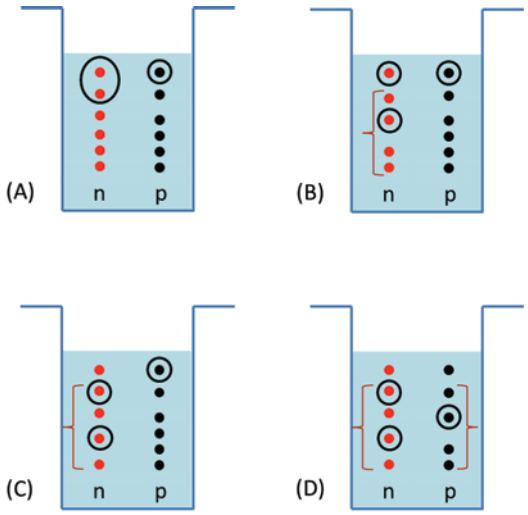

Figure 2. The class of the picked-up nucleons in direct (p, α) reactions; (A) the surface one, and (B) one neutron is from an inner orbit, (C) two neutrons are from inner orbits, and (D) all nucleons are chosen from inner orbits.

3 Results and discussion

To validate the proposed model, DDXs of (p, dx) and (p, αx) reactions were calculated and compared with experimental data. All the data used presently were obtained from the EXFOR data base [11].

3.1 (p, d) reactions

The solid and the dashed lines in Fig. 3 show the INC contributions of pickup from the surface and the inner orbits, respectively for the 42-MeV ^{27}Al(p, dx) reaction at laboratory angles of 30˚ and 60˚.

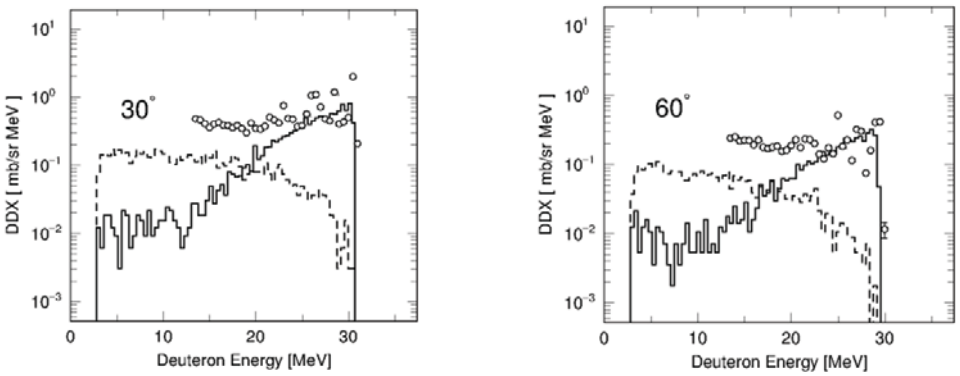

Figure 3. The INC contributions of the pickup from the surface orbit (solid line) and the inner orbits (dashed line) are shown for the ^{27}Al(p, dx) reaction at 42 MeV at laboratory angles of 30˚ (left) and 60˚ (right).

Open circles are experimental data. Since the experiments were conducted with detectors of poor energy resolutions, discrete levels were not very clear. Although data points distribute largely in the low excitation regions of these figures, average tendency is reproduced by solid lines, the surface pickup. The low-energy regions shown by the solid lines are due to rescattering of deuteron inside the nucleus. The pickup from inner-shells contributes to the flat shape spectra in the low-energy range.

In Fig. 4, spectral DDXs are compared between present calculation results and experiments for the same reaction as Fig. 3, in which solid lines and open circles indicate the calculation results and the experiments, respectively. Each calculation result is the sum of present INC (pickup from the surface and the inner orbits) and GEM for the evaporation. In experiments, evaporation regions were not observed due to the dead layers of detectors. Since experimental points show rising and falling due to the discrete level spectra reflected by the shell structure, there exist some discrepancies. However, the present calculations are in reasonable agreements with experimental data at four angles.

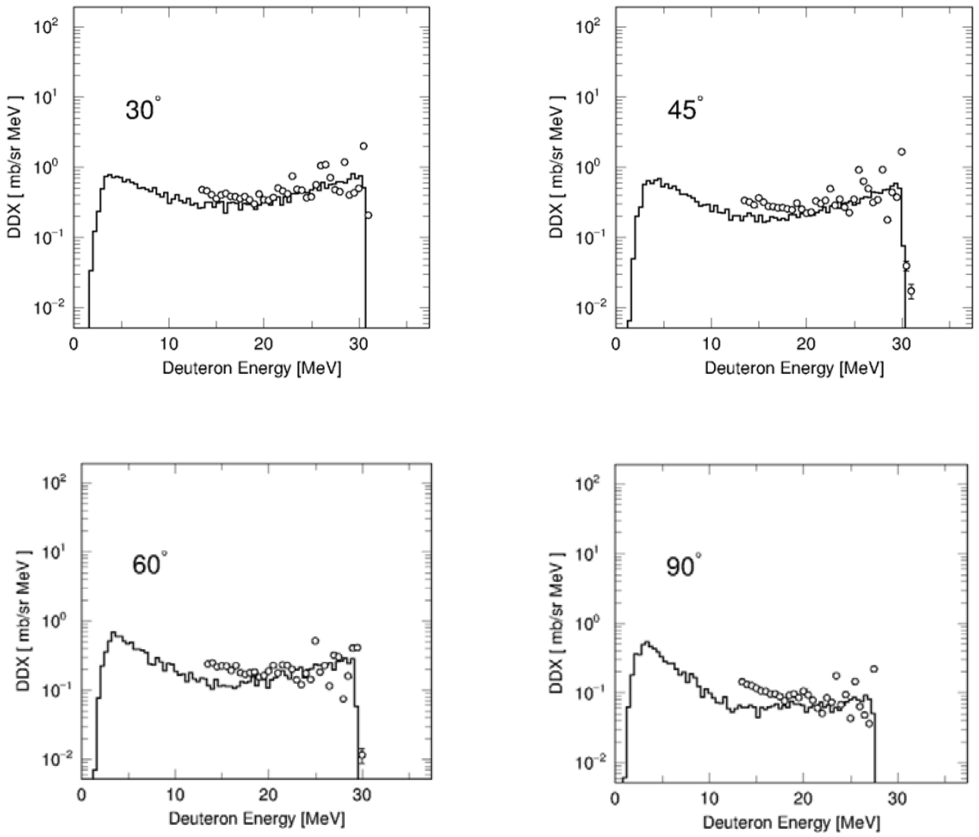

Figure 4. Comparison of double-differential cross sections (DDX) between present calculation (solid lines) and experiment (open circles) for the ^{27}Al(p, dx) reaction at 42 MeV. The calculation results include the evaporation components in addition to the total of the present INC (pickup from the surface and the inner orbits).

Figure 5 is the same as Fig. 3, but for the deuterons from the 42-MeV ^{58}Ni(p, dx) reaction. The experimental spectra in the low excitation regions are somehow sharper than those for ^{27}Al in Fig. 3. These experimental spectra are interpreted well by the calculation with the surface pickup model.

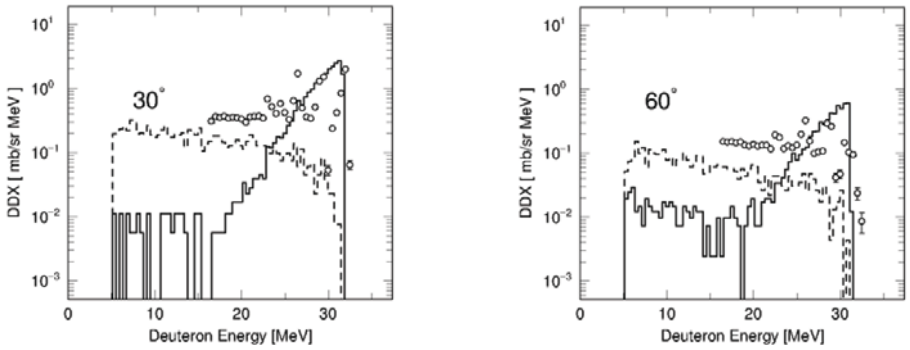

Figure 5. The contributions of the pickup from the surface orbit (solid line) and the inner orbits (dashed line) are shown for the ^{58}Ni(p, dx) reaction at 42 MeV at laboratory angles of 30° (left) and 60° (right).

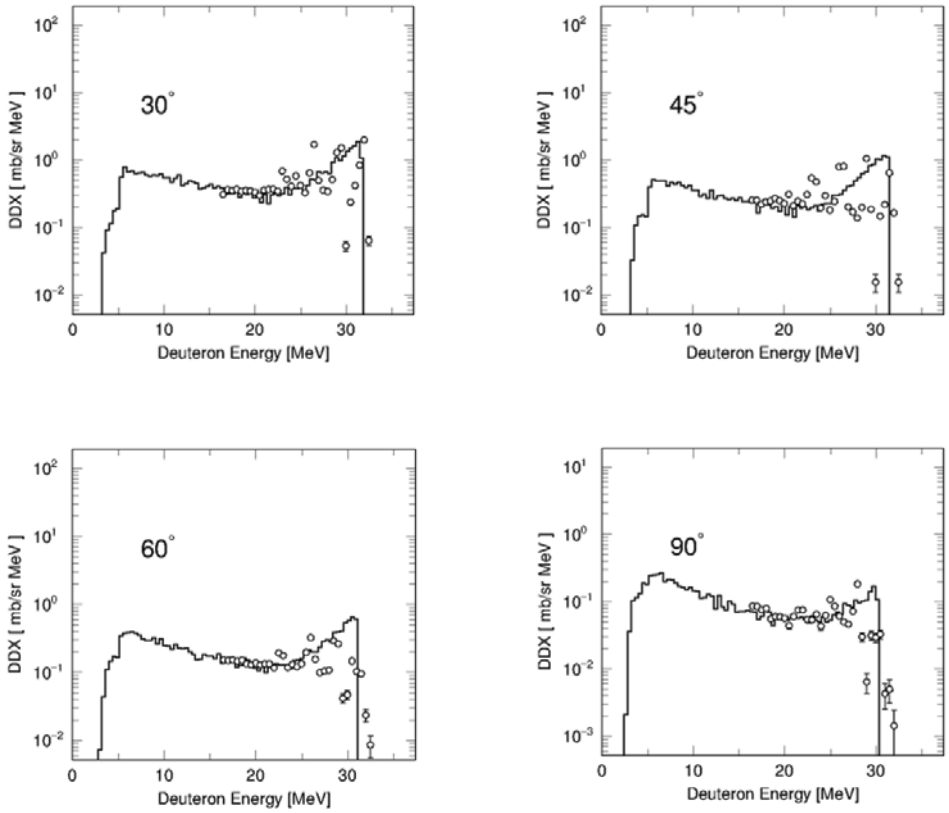

Figure 6. Comparison of double-differential cross sections (DDX) between present calculation (solid lines) and experiment (open circles) for the ^{58}Ni(p, dx) reaction at 42 MeV. The calculation results include the evaporation components in addition to the total of the present INC (pickup from the surface and the inner orbits).

Spectral DDXs for the ^{58}Ni(p, dx) reaction at 42 MeV are compared between present calculation and experiment in Fig. 6, which is the same as Fig. 4. As the case of the ^{27}Al target, reasonable agreements are observed between the present calculation and the experiment.

The present model was verified at the higher energy. Figure 7 is the same as Fig. 4 and 6, but for the ^{58}Ni(p, dx) reaction at 68 MeV. As in the case of the lower incident energy, present calculations are in reasonable agreements with the experiment.

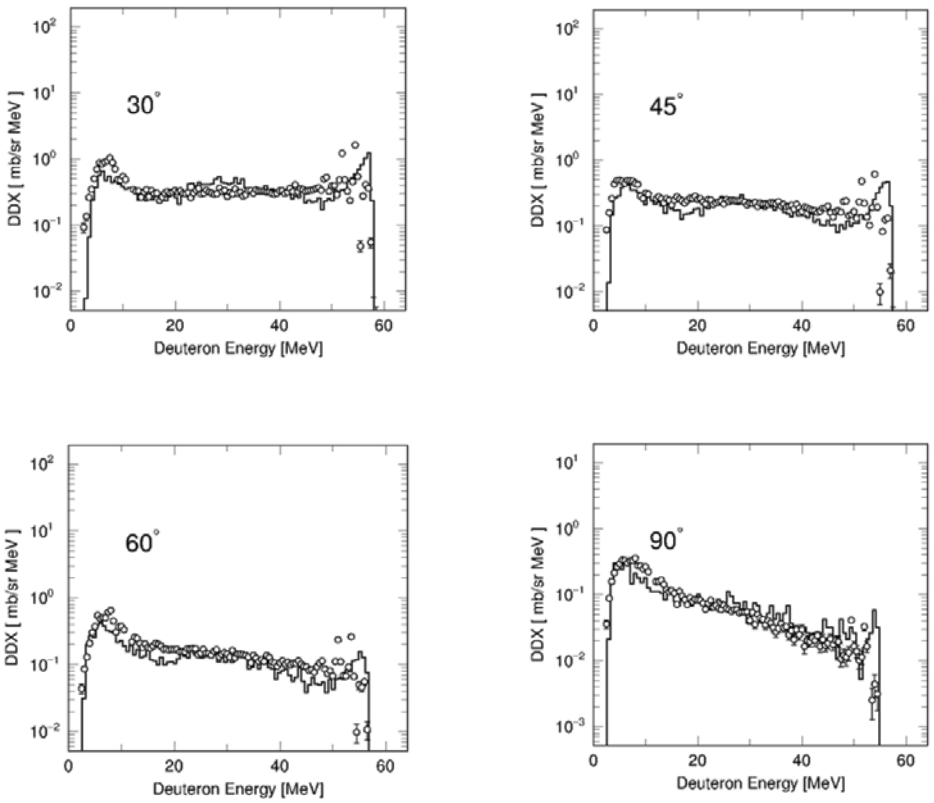

Figure 7. Comparison of double-differential cross sections (DDX) between present calculation (solid lines) and experiment (open circles) for the ^{58}Ni(p, dx) reaction at 68 MeV. The calculation results are the sum of the evaporation components and the present INC (pickup from the surface and the inner orbits).

3.2 (p, α) reactions

In Fig. 8, INC contributions of pickup from the surface and the inner orbits, which are discussed in Fig. 2, are displayed for the ^{58}Ni(p, αx) reaction at incident energies of 42 MeV (left) and 68 MeV (right) at laboratory angles of 30˚. At the higher incident energy, the contribution from the inner shell becomes more important. The surface pickup is responsible to the low excitation region and the inner-orbit pickup appears in the high excitation region. These results are consistent with understanding of the direct pickup mechanism.

Spectral DDXs of the ^{58}Ni(p, αx) reaction at 42 MeV are displayed in Fig. 9 at angles from 30˚ to 90˚, in which solid lines are the total of INC and GEM results, and dashed lines indicate GEM results only. As shown in Fig. 8, INC includes only two classes of pickup combinations at this incident

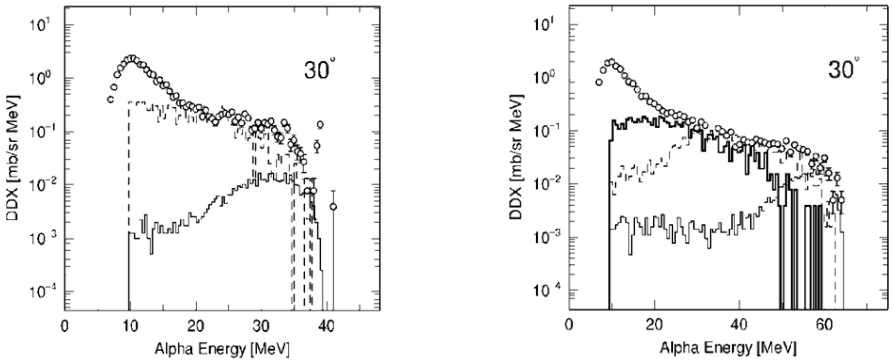

Figure 8. Contribution of each class of pickup of the present INC for ^{58}Ni(p, αx) reaction at incident energies of 42 MeV (left) and 68 MeV (right) at laboratory angles of 30˚. Thine, broken, and thick lines correspond to (A)-(C) of Fig. 2, respectively.

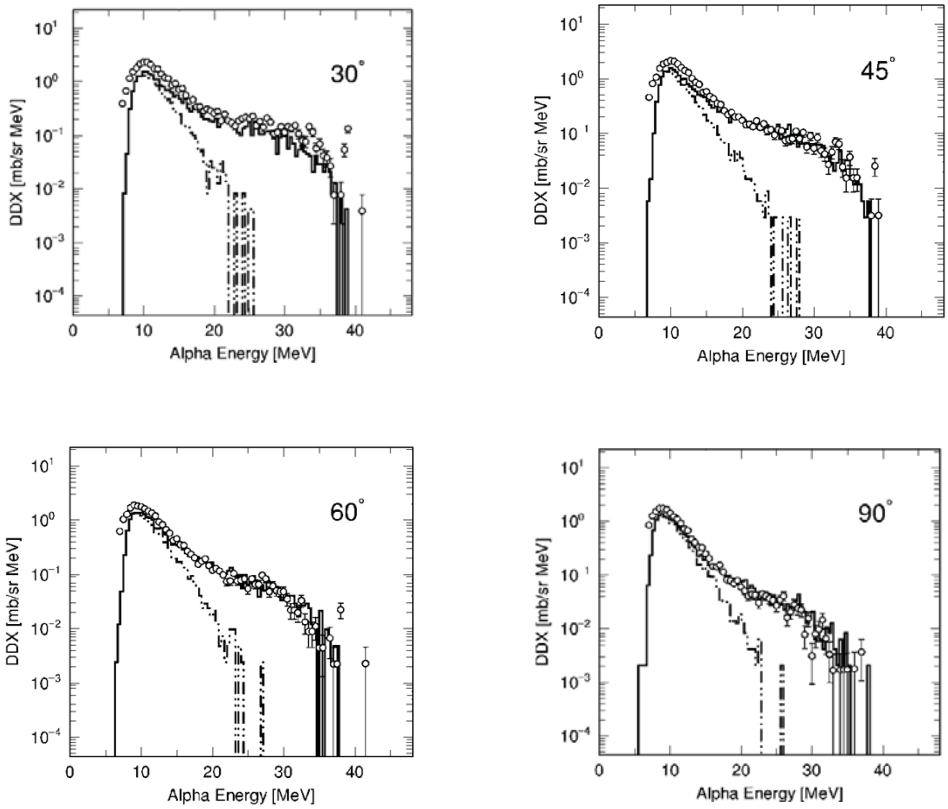

Figure 9. Comparison of double-differential cross sections (DDX) between present calculation (solid lines) and experiment (open circles) for the ^{58}Ni(p, αx) reaction at 42 MeV. The calculation results with solid lines include the evaporation components in addition to the total of the present INC (pickup from the surface and the inner orbits). Dashed lines indicate only the evaporation results.

energy. The experimental results show significant peaks, which come from the evaporation process, at around 10 MeV. With increasing the α energy, the experimental DDXs decrease gradually. This tendency is explained well by the present model. At the highest energy region, experiments show a few peaks and falling, which reflect the shell model structure of residual nuclei. Although the calculation model ignores the shell structure, calculation results are in reasonable agreements with the experiment. It should be stressed that the overall agreements are shown over the three-order changes in DDX magnitude at 90˚.

In Figs. 10 and 11 are shown DDXs for the (p, αx) reactions at 68 MeV on ^{58}Ni and ^{27}Al, respectively. At this incident energy, the INC calculations employed four classes of pickup combinations, which are shown in Fig. 2. Experimental spectra are very similar to those at 42 MeV except that the peak structures are not observed. Although slight discrepancies are indicated, overall close agreements are shown between the present model calculations and experiments.

The triton pickup probabilities were determined to fit experimental data in terms of pickup classes defined in Fig. 2. The resultant probabilities are shown in Fig. 12 on the target of ^{27}Al and ^{58}Ni as function of incident energy.

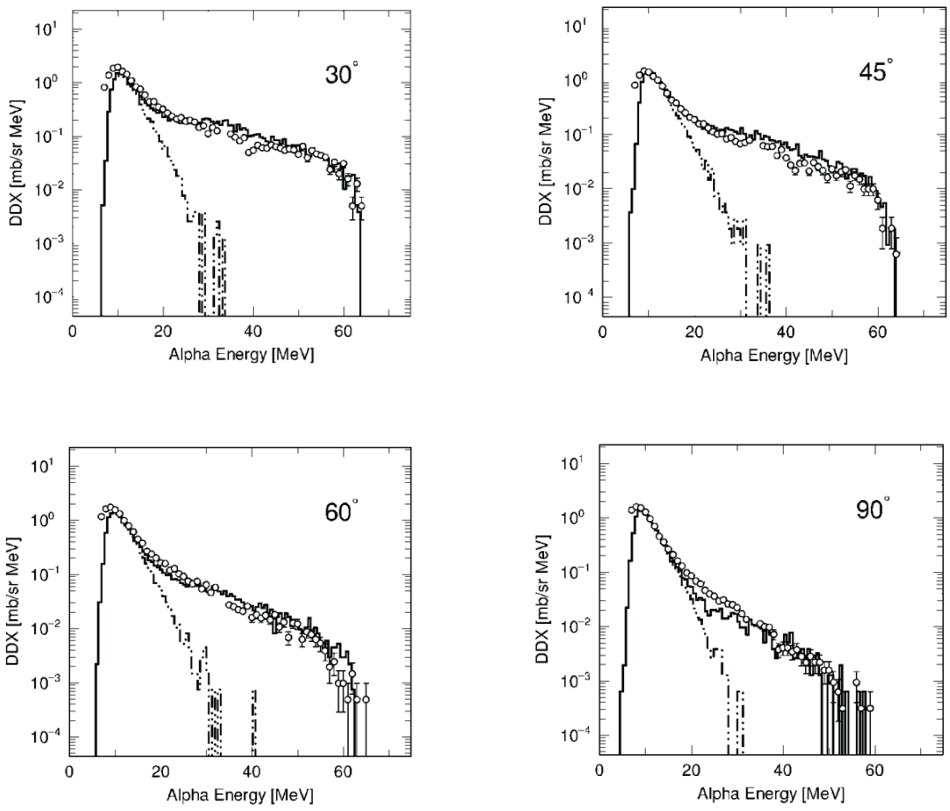

Figure 10. Comparison of double-differential cross sections (DDX) between present calculation (solid lines) and experiment (open circles) for the ^{58}Ni(p, αx) reaction at 68 MeV. The calculation results with solid lines include the evaporation components in addition to the total of the present INC (pickup from the surface and the inner orbits). Dashed lines indicate only the evaporation results.

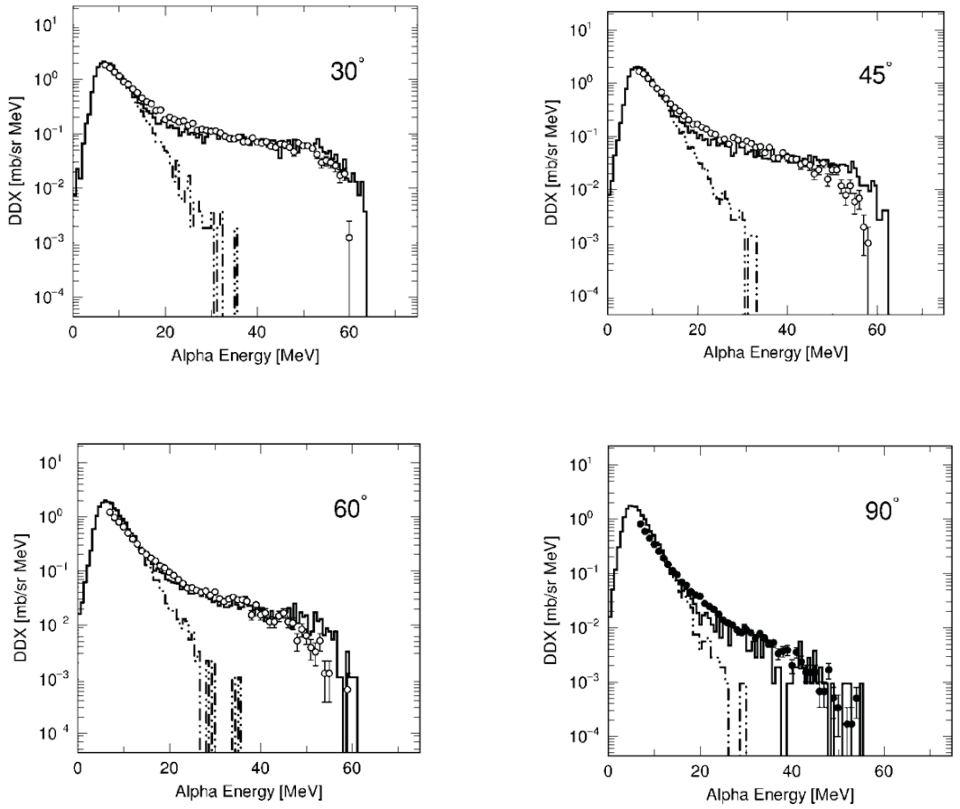

Figure 11. Same as Fig. 10, but for the ^{27}Al(p, αx) reaction at 68 MeV.

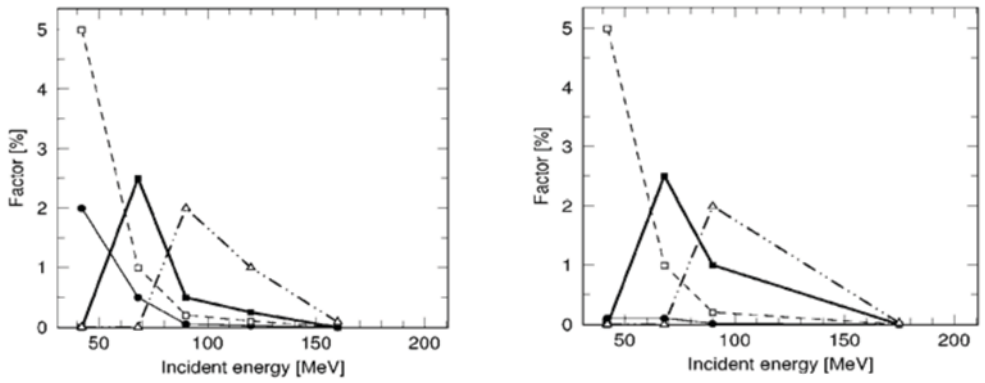

Figure 12. Factors of pickup probabilities for pickup classes of (p, αx) reactions on ^{27}Al (left) and ^{58}Ni (right) as function of incident energy. Dots, open squares, closed squares and open triangles show pickup classes shown in Fig. 2 (A) to (D), respectively.

3.3 (d, d'x) and (α, α'x) reactions

The present model to transport deuterons and α–particles inside the target nucleus was verified. Calculated DDXs for 80-MeV ^{27}Al (d, $d'x$) reactions are compared with experiments in Fig. 13, and the comparison for 140-MeV ^{27}Al(α, $\alpha'x$) reactions were displayed in Fig. 14. The observed angles are 30˚ and 90˚ for the both cases. Disagreements appear at the forward angle, where collective excitation process contributes significantly. At the large angle, the experimental magnitude variations over three-orders are interpreted successfully by the present model. Therefore, it is validated that the present model reproduces experimental data reasonably.

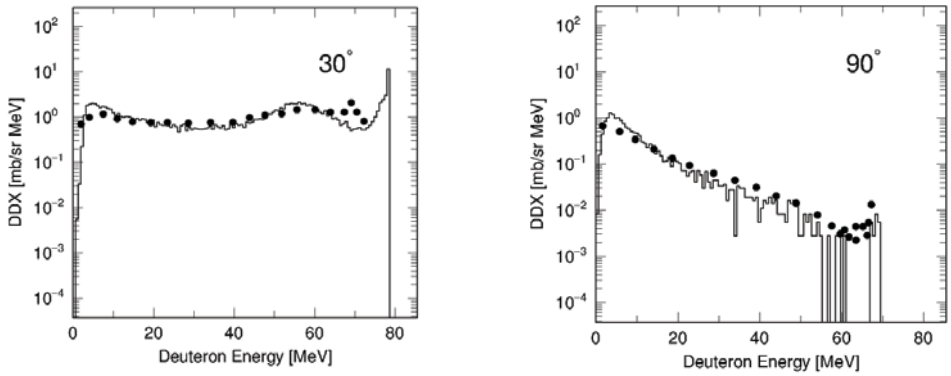

Figure 13. Comparison of double-differential cross sections (DDX) for the ^{27}Al(d, $d'x$) reaction at 80 MeV, at laboratory angles of 30˚ (left) and 90 ˚ (right). Solid lines are the calculation results including the evaporation components. Dots are experimental results.

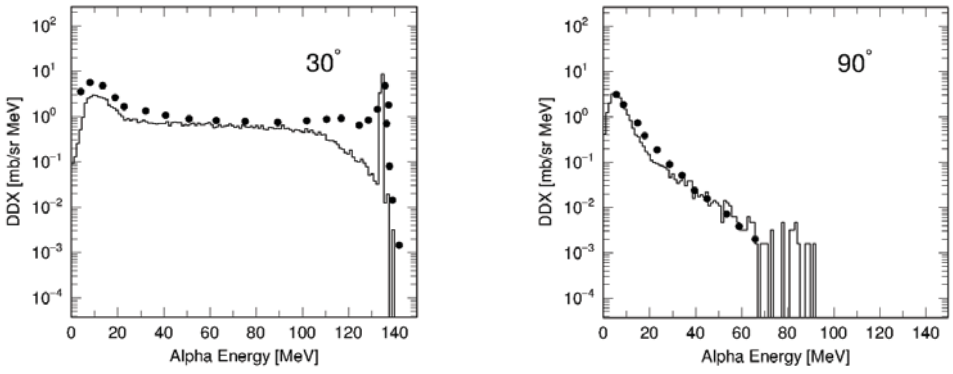

Figure 14. Comparison of double-differential cross sections (DDX) for the ^{27}Al(α, $\alpha'x$) reaction at 140 MeV, at laboratory angles of 30˚ (left) and 90 ˚ (right). Solid lines are the calculation results including the evaporation components. Dots are experimental results.

4 Conclusion

The Intranuclear Cascade (INC) model was extended to incorporate the direct pickup process to interpret (p, dx) and (p, αx) reactions at incident energies below 100 MeV, where the standard INC model has poor predictive ability. The proposed pickup model is based on a semi-classical interpretation of the nucleon transfer processes. In order to reproduce the whole energy range of emitted particles, possible classes of picked-up particles were introduced.

Calculations of the proposed model followed by the generalised evaporation model GEM were performed for (p, dx) and (p, αx) reactions on ^{27}Al and ^{58}Ni at incident energies of 40 and 68 MeV to be compared with experiments. Some of the experimental data distribute largely due to the reflection of the shell model structure, which was ignored in the model. However, the overall close agreements are confirmed.

References

1. H. Iwamoto, M. Imamura, Y. Koba, Y. Fukui, G. Wakabayashi, Y. Uozumi, T. Kin, Y. Iwamoto, S. Hohara, M. Nakano, Phys. Rev. C **82**, 034604 (2010).
2. Y. Uozumi, *Proceedings of the 2010 Symposium on Nuclear Data*, JAEA-Conf 2011-02, 65 (2011).
3. Y. Uozumi, Y. Sawada, A. Mzhavia, S. Nogamine, H. Iwamoto, T. Kin, S. Hohara, G. Wakabayashi, M. Nakano, Phys. Rev. C **84**, 064617 (2011).
4. Y. Uozumi, T. Yamada, S. Nogamine, M. Nakano, Phys. Rev. C **86**, 034610 (2012).
5. Y. Uozumi, T. Yamada, M. Nakano, Jour. Nucl. Sci. Tech. **52**, 264 (2015).
6. G. Montarou, J. P. Alard, J. Augerat, L. Fraysse, M. J. Parizat, R. Babinet, Z. Fodor, et al., Phys. Rev. C **44**, 365 (1991).
7. A. Boudard, J. Cugnon, J.-C. David, S. Leray, D. Mancusi, Phys. Rev. C **87**, 014606 (2013).
8. R. Bonetti, F. Crespi, K.-I.Kubo, Nucl. Phys. A **499**, 381 (1989).
9. S. Furihata and T. Nakamra, Jour. Nucl. Sci. Tech. **39**, Suppl. 2, 758 (2001).
10. J. Cugnon, D. L'Hote, J. Vandermeulen, Nucl. Instrum. Methods Phys. Res. B**11**, 251 (1996).
11. EXFOR Experimental Nuclear Reaction Data, https:// www-nds.iaea.org/exfor/exfor.htm.